HHS Public Access

Author manuscript

Adv Mater Technol. Author manuscript; available in PMC 2022 June 01.

Published in final edited form as:

Adv Mater Technol. 2021 June ; 6(6): . doi:10.1002/admt.202100162.

Conducting polymer-based granular hydrogels for injectable 3D cell scaffolds

Vivian Rachel Feig[#],
Department of Materials Science and Engineering, Stanford University, Stanford, CA, 94305, USA

Sruthi Santhanam[#],
Department of Neurology and Neurological Sciences, Stanford University School of Medicine, Stanford, CA, 94305, USA

Kelly Wu McConnell,
Department of Neurology and Neurological Sciences, Stanford University School of Medicine, Stanford, CA, 94305, USA

Kathy Liu,
Department of Materials Science and Engineering, Stanford University, Stanford, CA, 94305, USA

Matine Azadian,
Department of Neurology and Neurological Sciences, Stanford University School of Medicine, Stanford, CA, 94305, USA

Lucia Giulia Brunel,
Department of Chemical Engineering, Stanford University, Stanford, CA, 94305, USA

Zhuojun Huang,
Department of Materials Science and Engineering, Stanford University, Stanford, CA, 94305, USA

Helen Tran,
Department of Chemical Engineering, Stanford University, Stanford, CA, 94305, USA

Paul M. George[*],
Department of Neurology and Neurological Sciences, Stanford University School of Medicine, Stanford, CA, 94305, USA

Zhenan Bao[*]
Department of Chemical Engineering, Stanford University, Stanford, CA, 94305, USA

[#] These authors contributed equally to this work.

Abstract

[*]Corresponding authors who contributed equally: pgeorge1@stanford.edu, zbao@stanford.edu.

Supporting Information

Supporting Information is available from the Wiley Online Library or from the author.

Conflict of Interest

The authors report no competing interests.

Injectable 3D cell scaffolds possessing both electrical conductivity and native tissue-level softness would provide a platform to leverage electric fields to manipulate stem cell behavior. Granular hydrogels, which combine jamming-induced elasticity with repeatable injectability, are versatile materials to easily encapsulate cells to form injectable 3D niches. In this work, we demonstrate that electrically conductive granular hydrogels can be fabricated via a simple method involving fragmentation of a bulk hydrogel made from the conducting polymer PEDOT:PSS. These granular conductors exhibit excellent shear-thinning and self-healing behavior, as well as record-high electrical conductivity for an injectable 3D scaffold material (~10 S m^{-1}). Their granular microstructure also enables them to easily encapsulate induced pluripotent stem cell (iPSC)-derived neural progenitor cells, which were viable for at least 5 days within the injectable gel matrices. Finally, we demonstrate gel biocompatibility with minimal observed inflammatory response when injected into a rodent brain.

Graphical Abstract

Using a simple bulk fragmentation approach, electrically conductive granular hydrogels are fabricated that exhibit record-high conductivity for an injectable 3D scaffold material. These granular conductive hydrogels are able to encapsulate neural progenitor cells and be injected into a rodent brain with minimal observed inflammatory response.

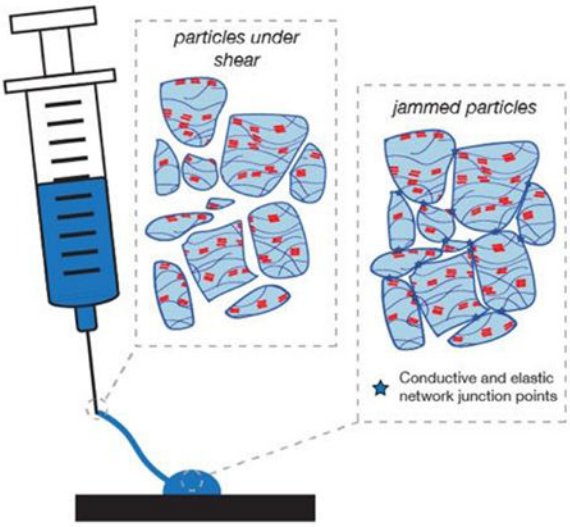

Keywords

conductive hydrogels; 3D cell scaffolds; injectable hydrogels

1. Introduction

Within the field of regenerative medicine, there is increasing interest in using electric fields to manipulate stem cells and enhance stem cell differentiation.[1–5] Electronically active scaffolds made of graphene[6] and conductive polymers such as polyaniline,[7] poly(3,4-ethylenedioxythiophene) (PEDOT),[8] and polypyrrole,[9,10] have been utilized to electrically stimulate neural stem cells to improve proliferation, neurite outgrowth,[7,8] and

cellular differentiation to neurons, astrocytes or oligodendrocytes.[1,11,12] However, the ability to leverage electrical functionalities is limited by an often-severe mismatch in mechanical properties between electronic materials and soft brain tissue, as neural stem cells are known to be highly sensitive to the mechanics of their surrounding environment.[2,13] Conductive hydrogels, which combine electrical conductivity with high water content, have emerged as promising materials to electrically interact with cells while maintaining desired tissue-like mechanical characteristics.[14–17]

Despite recent advances in bolstering the electrical and mechanical performance of these hydrogels,[15–18] limitations in the synthesis and delivery of electrically-functional regenerative therapies remain. While existing biocompatible conductive hydrogels can provide soft 2D interfaces for cells, 3D cell scaffolds better recapitulate the interactions between cells and their natural tissue environments.[19] Additionally, if such scaffolds are injectable, they will enable regenerative therapies to be delivered *in vivo* without requiring surgical procedures that pose high risks for complications like infection.[20] As such, next-generation biocompatible conductive scaffolds that can form injectable 3D conductive cell niches are highly desired.

To form an injectable and conductive 3D cellular niche, either the gelation process should be non-cytotoxic, or the scaffold material should be repeatably injectable to enable mixing with cells.[21–23] However, combining these design requirements with the need for high conductivity poses a significant challenge. This is because biocompatible gelation methods and the labile network junctions required for injectability are both often incompatible with the macroscopically connected conductive networks needed for electrical charge transport. Thus, existing reported conductive hydrogels used for 3D scaffolds that are potentially injectable exhibit poor conductivities, less than 10^{-1} S m^{-1} (Table S1). The most conductive injectable scaffold reported so far to our knowledge (~1.5 S m^{-1} in PBS) achieved this by crosslinking the conducting component into the macroscopic network.[24] Granular hydrogels, which derive elasticity from the jamming of concentrated microgel particles, may provide a route to circumvent these limitations.

Granular materials achieve injectability because jammed microparticles can flow past one another upon application of a shear or elongational stress.[25–27] In 2019, Shin and coworkers reported the first conductive granular hydrogel based on silver nanoparticles embedded within an insulating granular gel matrix.[27] While this was a promising demonstration of the potential for incorporating electrical functionality in granular materials, their conductivity was dependent on inorganic nanoparticle fillers, which can still pose problems with mechanical and chemical compatibility at the local bio-electronic interface.

In this work, we present the first injectable conductive granular hydrogel that is biocompatible in the neural environment. We present a simple approach for fabricating granular PEDOT:PSS hydrogels via fragmentation from a bulk conductive PEDOT:PSS gel. The electrical conductivity of the gel is achieved by leveraging the ability for the conducting polymer PEDOT:PSS to form hydrogel networks through **π-π** stacking interactions.[16,17,28,29] The granular materials formed from conductive PEDOT:PSS microgel building blocks exhibits both jamming-induced elasticity and conductivity, giving rise to an injectable

conductive gel. The injectable gel is biocompatible with neural stem cells as well as *in vivo* in the neural environment.

2. Results

2.1. Fabrication of conductive granular hydrogels

Conductive granular hydrogels are fabricated in a simple three-step process (Figure 1A). First, a colloidal gel is formed by mixing aqueous PEDOT:PSS solution with a concentrated (10x) phosphate buffered saline. The ions in the concentrated PBS solution screen the electrostatic repulsions between the negatively charged PSS-rich colloidal suspensions, enabling the dilute colloids to aggregate into a solid-like gel, as confirmed by tan delta values less than 1 in an oscillatory frequency sweep between 0.1 Hz and 10 Hz at 1% strain (Figure S1A). The solid-like nature of this colloidal gel enables the subsequent processing step, in which the gel is immersed in a solution of acetic acid to induce transition to an electrically conductive morphology (Figure S1B and S1C).

Immersing the PEDOT:PSS hydrogel in acetic acid transforms the material from an ionically conductive colloidal hydrogel to an electrically conductive hydrogel, as evidenced by the changes in impedance through the gel (Figure S1E). Impedance through a material is a measure of its frequency-dependent resistance to charge transfer. In a typical plot of the absolute value of impedance as a function of frequency, resistive behavior is characterized by frequency-independence, whereas capacitive behavior is characterized by a sharp frequency dependence. Ion-only conductors, like PBS solution, typically exhibit frequency-independent, resistive behavior at high frequencies, at which ionic species are able to behave like charge carriers. However, at lower frequencies, a sharp, frequency-independent increase in impedance is observed, indicative of capacitive behavior at low frequencies[30] (Figure S1D).

Before acetic acid treatment, the colloidal PEDOT:PSS hydrogel exhibits a similar frequency-dependent impedance profile as the PBS solution, suggesting its primary mode of charge transport is ionic (Figure S1E). On the other hand, acetic acid treatment results in an impedance spectrum exhibiting resistive behavior at all frequencies, suggesting the emergence of electronic charge carriers at low frequencies.[31,32] This dual conductivity is supported by the fact that the impedance decreases with acetic concentration, despite controlling for ionic concentration by neutralizing all gels thoroughly with PBS (Figure S1E). The emergence and enhancement of electronic conductivity with acetic acid treatment is consistent with previously reported fabrication methods for conductive PEDOT:PSS hydrogels that also leverage interactions between PEDOT:PSS and ionic species known to enhance conductivity in PEDOT:PSS thin films by promoting phase separation of PEDOT from PSS, including certain ionic liquids[17] and acids[28] (Figure S2). We chose acetic acid because it is biologically benign compared to these other reported ionic species,[33] in case any residual acid remains after neutralization with PBS.

In the final step, a granular microstructure is obtained by fragmenting the conductive hydrogel with vigorous stirring. Application of a shear stress to the hydrogel results in a microstructure that is, by its nature, sufficiently granular to behave like a mixable liquid at

that stress (Figure 1B). Since stirring alone cannot re-solubilize the polymers, the fragmented material behaves like a jammed collection of microparticles, in which elasticity emerges due to the caging of each particle by its nearest neighbor (Figure 1C). As no additional solvent is introduced, the resulting granules are inherently space-filling, ensuring a high packing density. Bulk fragmentation results in random, heterogeneous microparticles with equivalent circular diameters (ECD) ranging from tens to hundreds of microns (Figure 1D and S3).

Critically, all particles had ECD values smaller than the inner diameter of a standard 26 gauge needle (260 μm), with 99.33% of particles smaller than 120 μm. Lyophilization and subsequent imaging with a scanning electron microscope also confirm that the fragmented granular gel retains a porous nature (Figure 1E).

2.2. Rheological properties were consistent with an injectable jammed granular material

Fragmentation results in a slight decrease in storage modulus (G') compared to the bulk gel (Figure 2A), which is expected since flow necessitates breaking some macroscopic crosslinks. Nevertheless, the fragmented hydrogel retains elasticity at low strains, with similar tan delta values as the bulk gel: less than 1 in the 0.1 Hz to 10 Hz frequency range at 1% strain (Figure 2A). The fragmented gel exhibits excellent shear-thinning behavior, with a power law index of 0.0501 (Figure 2B). Additionally, the fragmented gel's dynamic yield stress of 1.9 kPa (Figure 2B) is well below reported maximum applicable pressures for health personnel, which are at least 131 kPa depending on the syringe volume.[34]

Oscillatory rheometry suggests that this macroscopic behavior can be attributed to a granular microstructure. In an oscillatory amplitude sweep, the material exhibits a clear transition from solid-like (G'> loss modulus, G") to liquid-like (G">G') behavior at a strain of around 15% (Figure 2C), indicating that low shear strains can sufficiently disrupt network junctions to enable flow. This is unsurprising for a granular material, in which elasticity arises from relatively weak frictional forces between jammed particles, especially compared to other supramolecular crosslinks like metal-ligand coordination bonds. The peak in the loss modulus (G") curve near the transition point is also consistent with energy dissipation via jammed microparticle rearrangement[35,36] (Figure 2C). The fragmented gel can quickly and reversibly alternate between liquid-like behavior at high strains (500%) and solid-like behavior at low strains (1%), consistent with other granular systems[26,27] (Figure 2D). Taken together, these rheological characteristics enable the gel to be injected by hand through both a 20 gauge (603 μm diameter) (Figure 2E) and a 26 gauge (260 μm diameter) needle (Figure S4A), and to rapidly recover its solid-like properties after injection (Figure 2F and S4B).

2.3. Granular gels exhibited low impedances at all frequencies arising from their jammed microstructure

AC impedance was used to characterize the charge-carrying properties of the fragmented gel because it can decouple electronic from ionic effects. This is particularly important for our system, which comprises mobile charged species (including, potentially, the microparticles). After fragmentation, there was a slight increase in the frequency-dependent impedance

through the material at all frequencies (Figure 3A and 3B), which is consistent with the fact that many of the broken bonds are expected to be conductive π-π stacking network junctions.

Interestingly, the increase is minimal, especially compared to the dramatically higher low-frequency impedances of an only-ionically conductive control (1x PBS solution) (Figure 3A). Crucially, the relatively frequency-independent profile of the bulk gel is maintained (Figure 3A). Since fragmentation into a granular state results in large microparticles, it appears that a large portion of the π-π stacking interactions formed by the acid treatment step is maintained. The breaking of bonds may also be somewhat compensated by an improved interfacial resistance between the granular gel and the planar measurement electrodes, which is evidenced by the fact that the impedance of the granular gels, as compared with bulk gels, gradually decreases over time until it reaches an equilibrium value (Figure S5). This relaxation rate correlates well with the decrease in axial force upon loading the granular gels on a parallel plate rheometer (Figure S5), suggestive of an interfacial relaxation process.

Further supporting the presence of electrical conductors in the granular gel, application of a constant DC voltage of 0.1V resulted in a persistent current flow of 32.9 mA (Figure 3C), equating to a conductivity of 10.8 S m^{-1}. Over 3 samples, the granular gels exhibited an average conductivity of 8.4 S m^{-1} with a standard deviation of 2.9 S m^{-1}; this variability is a limitation of the fragmentation method of synthesizing granular gels, which we address in more detail in the Conclusion section. By contrast to the granular gels, the colloidal PEDOT:PSS hydrogel, which does not have the acid-induced electrically conductive morphology, shows a rapid decay in current (Figure 3C). Finally, to prove that the low impedances of our material are not purely an interfacial phenomenon, impedance at various gap sizes between the electrodes was measured. As expected for a resistor, the impedance increased as gap size increased (Figure 3D); purely interfacial improvements, by contrast, would be independent of gap size.

To more directly correlate these electrical properties to their granular microstructure, we used electrically conductive parallel plates to perform oscillatory rheology on our gels while monitoring the electrical resistance of the circuit with a digital multimeter. Remarkably, the electrical resistance can be reversibly increased and lowered at high and low strains, respectively (Figure 3E). The inversely correlated relationship between the storage modulus and electrical resistance support our hypothesis that the jamming-induced elasticity of the granular structure also gives rise to percolating electrical conduction. Finally, because the electrical network forms along with the elastic network, and both form rapidly after release of high shear stress, printing the material to complete a circuit comprising an LED leads the LED to light up immediately (Movie S1 and Figure 3F).

2.3. The injectable granular gels were biocompatible with cells and in rodents

The toxicity of the conductive hydrogels was determined using cell viability assays *in vitro* and *in vivo* in a rodent brain. Injectable conductive hydrogels were either used as-made or after pre-mixing with a cellulosic binding polymer, phenyl-modified hydroxymethylpropylcellulose (HPMC), in order to reduce erosion in cell culture media

(Supplementary Discussion 1), though we do not expect this binder to be needed for injection into regions of the body like brain tissue, which provides a confined space to hold the granular gel in place. An optimum ratio of 9:1 wt:wt conductive gel:HPMC was selected because it sufficiently prevented erosion *in vitro* while maintaining injectability and minimally increasing the impedance of the gel mixture (Figure S6).

For *in vitro* studies, injectable granular gels were mixed with human induced pluripotent stem cell (iPSC)-derived neural progenitor cells (NPC). The Live/dead assay illustrated that NPCs were viable when encapsulated in both PEDOT:PSS gels and PEDOT:PSS/HPMC gels on day 2 (Figure 4A). Percentage viability was determined as the ratio of total area with green fluorescence to that of total fluorescence (green and red). Although PEDOT:PSS/HPMC gels were found to be more compatible compared to PEDOT:PSS gels alone, there was no significant difference between the groups ($p=0.1725$, two-tailed t-test) (Figure 4B). To evaluate the proliferation of cells encapsulated within the gel matrices, we performed alamarBlue assay for days 1, 2 and 5 (Figure 4C). Cells encapsulated within both types of gels were found to be viable for up to 5 days without any significant difference compared to the positive control (cells on a Matrigel^{R} Matrix substrate). The cells within the PEDOT:PSS gel were at least 90% viable by day 5. Moreover, the percentage viability on day 2 was comparable to that of the live/dead assay. Cells in both gel matrices were viable without any significant difference between the two assays, when analyzed using a two-way ANOVA (Figure S7). The cytocompatibility of the granular gels were also comparable to other conductive scaffolds (Table S2). Overall, the *in vitro* assays demonstrated that both injectable conductive gel matrices were non-toxic to human NPCs.

To evaluate the toxicity of the gel *in vivo*, we injected 4 μL of gel per animal at four different coordinates in the rat brain (1 μL per site) using a stereotactic syringe injector. The experimental groups were injectable PEDOT:PSS and PEDOT:PSS/HPMC gels, while the control was a needle tract without any injection (N=4). In all treatments, the rats recovered after injection without any signs of pain or distress. They were sacrificed on day 7 and their brains were extracted, fixed, and sliced for immunostaining.

When a foreign body is introduced in the cortex of the brain, the inflammatory response is the first sign to indicate the toxicity of the foreign material. The biocompatibility of the gels were evaluated by staining for key components of the nervous system's response to implanted materials – microglia and astrocytes [37,38] (Figure 5). Microglia are first responders to the introduction of foreign material, and they accumulate and proliferate near the material starting immediately. On the other hand, astrocytes are activated by the microglial signaling and are prominent within a week after introducing the material. Hence, 7 days is an optimal time point to evaluate the acute toxicity of the material, and is also probably the most critical period for stem cell transplants. The brain slices were stained for glial fibrillary acidic protein (GFAP) – a type III filament protein that is expressed by astrocytes and indicative of gliosis. Additionally, immunofluorescent staining for the ionized calcium binding adaptor molecule 1 (Iba1) – a calcium specific protein specific to microglia/macrophages, was performed. The inflammatory response to the gels and the control were evaluated at two regions: (1) near the injection site and (2) tissue from the ipsilateral cortex approximately 500 μm away from the injection site, referred to as peri-injection site. The

astrocytes and microglia cells surrounding both the hydrogels were comparable to that of the needle tract control (Figure 5A). Moreover, the injected gels were well-formed within the tissue (Figure S8). Quantifying the percent area under fluorescence for inflammatory cells revealed that there was no significant difference in the microglia and astrocytes' accumulation near the gel compared to that of the control (Figure 5B and 5C). Together, the results reveal that the inflammatory response elicited by both gels is similar to that of the control and attributable to transient introduction of a foreign body. Hence, the granular gel was demonstrated to be non-toxic to brain tissue.

3. Conclusion

We have developed a next-generation conductive granular hydrogel that is injectable and biocompatible in the neural environment. The unique microstructure of granular conductive hydrogels makes them promising materials in regenerative medicine that involves electric field manipulation. Jamming of conductive microgel particles induces both macroscopic elasticity and conductivity, while the absence of chemical crosslinks between these particles makes them injectable via rapid shear-thinning and self-healing. The easy mixability of the gel with stem cells and their biocompatible nature make them an ideal candidate to form conductive 3D cellular niches.

PEDOT-based conductive gels are widely used to interact with stem cells because of their controllable gel properties[39,40] and cellular biocompatibility.[11,41] We have demonstrated that a simple "top-down" bulk fragmentation method is sufficient to generate PEDOT:PSS gels with a granular microstructure and thus create injectable conductive hydrogels with tissue-level elastic moduli (~ 1 kPa) and excellent conductivity (~10 S/m). We also found the granular PEDOT:PSS hydrogel to be cyto-compatible with the iPSC derived neural progenitor cells (60 – 90% viable). This cytocompatibility is comparable to the cytocompatibility of other conductive scaffolds used in neural and regenerative medicine (Table S2). The *in vivo* rodent studies demonstrated the injectability of the granular hydrogel through a 260 μm diameter needle as well cytocompatibility with the adjacent brain tissue, making it suitable for neural tissue regeneration treatments for injuries such as stroke, peripheral nerve injury and traumatic brain injury.

Future work may seek to address some of the limitations of bulk fragmentation by using alternate "bottom-up" methods for fabricating granular hydrogels, including microfluidic generation of individual microgel particles.[25] Bulk fragmentation results in variable material characteristics due to the inhomogeneity of the resultant microparticles, which also makes it difficult to systematically establish structure/property relationships. Moreover, fragmentation inevitably results in the elimination of some conductive network junctions when crosslinks are broken. Alternative approaches that maximize the conductivity of each individual microgel building block can potentially circumvent this and further boost the macroscopic conductivity of the granular gel. Finally, the porous nature of the microgel building blocks can be leveraged to increase complexity. For example, we previously demonstrated that secondary polymer networks can be interpenetrated with PEDOT:PSS hydrogels to orthogonally tune mechanical properties like stretchability and elastic modulus.[17] Since PEDOT:PSS hydrogels comprise the building blocks of our granular conductors,

we anticipate that interpenetrating polymer networks can similarly be used to orthogonally introduce functionalities like stabilization against erosion and stimuli-responsive behaviors. The potential to further improve on already strong electrical and injectable properties make granular PEDOT:PSS hydrogels a promising materials platform for next-generation conductive cell scaffolds for neural recovery.

4. Experimental Methods

Materials:

PEDOT:PSS Orgacon ICP1050, a surfactant-free aqueous dispersion with 1.1 wt% solid content, was provided by Agfa. Phosphate buffered saline (PBS) solutions at pH 7.4 were purchased from E&K Scientific Products.

Synthesis of bulk and granular conductive hydrogels:

Colloidal PEDOT:PSS hydrogels were first formed by mixing 90 vol% PEDOT:PSS solution with 10 vol% of concentrated (10x) PBS. Conductive bulk PEDOT:PSS hydrogels were formed by immersing colloidal gels in an acetic acid solution for 24 hours at a volume ratio of 1.2:1 acetic acid solution to gel. Subsequently, the gels were neutralized with repeated rinses in 1x PBS. Granular hydrogels were formed via fragmentation of the bulk conductive gel using a stir bar for 12 hours at 1000 rpm.

Structural characterization of granular hydrogels:

Optical microscopy was used to analyze the size distribution of sheared PEDOT:PSS particles dispersed in water. The open-source software, Fiji, was used to calculate surfaces areas of all PEDOT:PSS particles in 7 samples of the same PEDOT:PSS particle dispersion, totaling 451 particles. Only particles larger than 1 μm were measured, as smaller sizes were difficult to resolve with optical microscopy and can also be assumed to safely pass through any standard gauge needle. The equivalent circular diameter (ECD) was calculated for each particle by assuming that each irregularly shaped particle can be represented as a circle of the same surface area. Scanning electron microscopy was performed on lyophilized samples using a FEI Magellan 400 XHR Scanning Electron Microscope. X-ray photoelectron spectroscopy was performed on dried samples using a PHI Versaprobe III Scanning XPS Microprobe.

Characterization of rheological properties:

Both oscillatory and shear rheology measurements were performed using a TA Instruments ARES-G2 rheometer with a 25 mm parallel plate. Steady shear measurements were taken from high to low shear rate. Power law index, n, was calculated from the equation $\eta = \dot{\gamma}^{n-1}$, where η is viscosity and $\dot{\gamma}$ is shear rate; for shear thinning fluids, 0<n<1, where a value closer to 0 indicates more shear thinning. The ARES-G2's dielectric thermal analysis accessory (DETA) was used to simultaneously monitor electrical resistance while performing rheological measurements by connecting its conductive 25 mm parallel plates to a handheld digital multimeter. To account for variability in the fragmentation process, comparisons were only drawn between measurements made on the same batch of material.

For instance, to assess the impact of binding polymers on the material's rheological properties, the same PEDOT:PSS gel was used for measurements before and after incorporating additives.

Characterization of electrical properties:

Electrochemical impedance spectroscopy (EIS) and chronoamperometric (CA) measurements were performed using a Bio-Logic VSP potentiostat. For the EIS measurements, an AC voltage of amplitude 10 mV was applied. For the CA measurements, a DC voltage of 0.1V was applied. Samples were measured in a homemade cell comprising two electrodes made by evaporating 40 nm Au on 3 nm Cr on glass slides. A rubber spacer separated the electrodes, and samples were loaded into a cylindrical hole (diameter = 0.4375 inches) punched out from the rubber. Unless otherwise specified, rubber spacers were 0.125 inches thick. Cells were assembled and sealed with a paperclip, which was kept consistent between measurements to ensure uniform pressure, and equilibrated for up to 12 hours until measured values were steady. Impedance spectra for the granular gels were averaged over 4 samples. DC conductivity values were averaged over 3 samples and calculated using the equation $\sigma = L\ R^{-1}A^{-1}$, where L is the spacer thickness, $R=V\ I^{-1}$, and A is the hole diameter. To account for variability in the fragmentation process, comparisons were only drawn between measurements made on the same batch of material. For instance, the same batch of granular gel was used to assess the impact of spacer thickness on impedance properties.

Cytocompatibility studies:

The cytocompatibility of the granular hydrogel in contact with the human iPSC derived neural progenitor cells (NPC) was determined using the cell-viability assays - live/dead and alamarBlue assay. The NPCs were differentiated from iPSCs as described previously.[42] The NPCs (P5, about 30,000 cells/sample) were mixed with the granular gel particles and injected on-to sterile coverslips for the live/dead assay (N=3 per group) and a 24-well plate for the alamarBlue assay (N=4 per group). The cell-gel samples were left un-disturbed at room temperature for 30 mins and then maintained in NPC cell culture media at 37 °C. For the live/dead assay on day 2, the samples were incubated with ethidium homodimer-1 and calcein AM (2 μL mL^{-1} of 1x PBS; Thermo Fisher Scientific) for 15 mins at 37 °C. After incubation, the cells were rinsed with 1x PBS, and imaged using a fluorescent microscope (Keyence BZ-X700). Three images were obtained at different parts of the gel. The images were quantified for total area under fluorescence after thresholding the background using ImageJ. The triangle thresholding was chosen for green and intermodes for red fluorescence. The percentage viability was measured as the percent ratio of green over total fluorescence (green and red).

For the alamarBlue assay, the samples were immersed in a 10% alamarBlue™ cell viability reagent (Thermo Fisher Scientific) and incubated at 37 °C for 3 hours in the dark. The controls were cells without gel encapsulation (positive control) and cells incubated with cell lysis buffer (100 μL mL^{-1} of 1x PBS; Cell Signaling Technologies) for 1 hour prior to the assay (negative control). The absorbance of about 200 μL per sample were measured at 570 and 600 nm using a multi-plate reader (SpectraMax, Molecular Devices). The percentage

reduction in absorbance (percentage viability) was calculated with respect to the positive control – cells without encapsulation as per the manufacture protocol.

In vivo biocompatibility of gels:

All animal procedures were approved by Stanford University's Administrative Panel on Laboratory Animal Care (protocol number 31909). Adult male Sprague Dawley rats (275-300g) were anesthetized, administered with buprenorphine (0.5 mL per 100 g weight), and their surgical site was sterilized thrice using alternate betadine and ethanol wipe. The surgically prepped animals were then placed on a stereotaxic frame for gel injections. The scalp was incised, and 4 μL of the injectable conductive hydrogel was injected at four different coordinates in the brain (1 μL per site; mediolateral (ML) −2.4, dorsoventricular (DV) −2.4, injection #1: anteroposterior (AP) +2.5; #2: AP +1.5, #3: AP −1.0, #4: AP −2.0 with respect to bregma) using a syringe injector (26G needle). The incision was closed with monofilament sutures and the rodents were placed in a separate chamber for recovery. The experimental group were animals injected with PEDOT:PSS gel and PEDOT:PSS/HPMC gel, and the control was animals with needle tract without any injection (N=4 each). The rodents were continuously monitored post-injection for weight and other signs of stress or pain.

Immunostaining of brain tissues:

Animals were perfused on day 7 post-injection and 40 μm thick slices were sectioned using a cryostat. The brain slices (40 μm thickness, 400 μm apart, N=3-4 per brain) were stained for inflammatory cell markers – astrocytes (GFAP), and microglia (Iba1) as described.[42] Primary antibodies – anti-GFAP (1:500, MilliporeSigma), Iba 1 (1:500, MilliporeSigma) were incubated at 4 °C overnight. Secondary antibodies (Thermo Fisher Scientific) – Alexa Fluor 488 (1:500), 555 (1:500) were incubated for 2 hours followed by Hoechst solution (1:2000) for 5 mins at room temperature. The slices were imaged at the injection and peri-injection site using a fluorescent microscope (Keyence BZ-X800). Each image was quantified for percent area under fluorescence using ImageJ (NIH). The images were converted to 8-bit and thresholded using default method at 10-20% of histogram for GFAP and 5-6% for Iba1. Three regions of interest (0.01 mm^2 each) were selected randomly for peri-injection site and those closest to the gel/needle tract for injection site. The area under fluorescence were measured using particles analyzer for a circularity of 0-1 for Iba1 and 0-0.4 for GFAP and graphed using prism8 (GraphPad). Imaging and processing were performed by blinded individuals.

Statistical analysis:

All data are represented as Mean ± Standard deviation (SD). N is the number of individual samples. The data from live/dead assay was analyzed using an unpaired two-tailed t-test and from alamarBlue assay were analyzed via a mixed-effects model followed by a Turkey's statistical hypothesis testing for multiple comparisons. The *in vivo* data was analyzed using a nested-1-way ANOVA, followed by multiple comparison using Turkey's statistical hypothesis testing.

Supplementary Material

Refer to Web version on PubMed Central for supplementary material.

Acknowledgements

The authors thank Agfa for providing PEDOT:PSS ICP 1050, and Dr. Anthony Yu for providing the HPMC derivatives. This work was supported by a Big Ideas in Neuroscience grant from the Wu Tsai Neurosciences Institute at Stanford University. Part of this work was performed at the Stanford Nano Shared Facilities (SNSF), supported by the National Science Foundation under award ECCS-1542152. V.R.F. was supported by the Department of Defense (DoD) through the National Defense Science and Engineering Graduate (NDSEG) Fellowship Program. The work was supported by National Institutes of Health Grants K08NS089976 (to P.M.G.). V.R.F. and S.S. contributed equally to this work.

References

[1]. da Silva LP, Kundu SC, Reis RL, Correlo VM, Trends Biotechnol. 2020, 38, 24. [PubMed: 31629549]

[2]. Burnstine-Townley A, Eshel Y, Amdursky N, Adv. Funct. Mater 2019, 30, 1901369.

[3]. Gajendiran M, Choi J, Kim SJ, Kim K, Shin H, Koo HJ, Kim K, J. Ind. Eng. Chem 2017, 51, 12.

[4]. Oh B, Levinson A, Lam V, Song S, George P, J. Vis. Exp 2018, 134, e57367.

[5]. Oh B, George P, Brain Res. Bull 2019, 148, 10. [PubMed: 30851354]

[6]. Das SR, Uz M, Ding S, Lentner MT, Hondred JA, Cargill AA, Sakaguchi DS, Mallapragada S, Claussen JC, Adv. Healthc. Mater 2017, 6, 1601087.

[7]. Zarrintaj P, Urbanska AM, Gholizadeh SS, Goodarzi V, Saeb MR, Mozafari M, J. Colloid Interface Sci 2018, 516, 57. [PubMed: 29408144]

[8]. Wang S, Guan S, Wang J, Liu H, Liu T, Ma X, Cui Z, J. Biosci. Bioeng 2017, 123, 116. [PubMed: 27498308]

[9]. George PM, Bliss TM, Hua T, Lee A, Oh B, Levinson A, Mehta S, Sun G, Steinberg GK, Biomaterials 2017, 142, 31. [PubMed: 28719819]

[10]. Song S, Amores D, Chen C, McConnell K, Oh B, Poon A, George PM, Sci. Rep 2019, 9, 19565. [PubMed: 31863072]

[11]. Wang S, Guan S, Xu J, Li W, Ge D, Sun C, Liu T, Ma X, Biomater. Sci 2017, 5, 2024. [PubMed: 28894864]

[12]. Wang S, Guan S, Li W, Ge D, Xu J, Sun C, Liu T, Ma X, Mater. Sci. Eng. C 2018, 93, 890.

[13]. Vedadghavami A, Minooei F, Mohammadi MH, Khetani S, Rezaei Kolahchi A, Mashayekhan S, Sanati-Nezhad A, Acta Biomater. 2017, 62, 42. [PubMed: 28736220]

[14]. Yuk H, Lu B, Zhao X, Chem. Soc. Rev 2019, 48, 1642. [PubMed: 30474663]

[15]. Liu Y, Liu J, Chen S, Lei T, Kim Y, Niu S, Wang H, Wang X, Foudeh AM, Tok JBH, Bao Z, Nat. Biomed. Eng 2019, 3, 58. [PubMed: 30932073]

[16]. Lu B, Yuk H, Lin S, Jian N, Qu K, Xu J, Zhao X, Nat. Commun 2019, 10, 1043. [PubMed: 30837483]

[17]. Feig VR, Tran H, Lee M, Bao Z, Nat. Commun 2018, 9, 2740. [PubMed: 30013027]

[18]. Sasaki M, Karikkineth BC, Nagamine K, Kaji H, Torimitsu K, Nishizawa M, Adv. Healthc. Mater 2014, 3, 1919. [PubMed: 24912988]

[19]. Santos E, Hernández RM, Pedraz JL, Orive G, Trends Biotechnol. 2012, 30, 331. [PubMed: 22560988]

[20]. Quinn TD, Brovman EY, Aglio LS, Urman RD, Clin. Neurol. Neurosurg 2017, 161, 6. [PubMed: 28772171]

[21]. Mironi-Harpaz I, Wang DY, Venkatraman S, Seliktar D, Acta Biomater. 2012, 8, 1838. [PubMed: 22285429]

[22]. Spicer CD, Polym. Chem 2020, 11, 184.

[23]. Talebian S, Mehrali M, Taebnia N, Pennisi CP, Kadumudi FB, Foroughi J, Hasany M, Nikkhah M, Akbari M, Orive G, Dolatshahi-Pirouz A, Adv. Sci 2019, 6, 1801664.

[24]. Xu Y, Patsis PA, Hauser S, Voigt D, Rothe R, Günther M, Cui M, Yang X, Wieduwild R, Eckert K, Neinhuis C, Akbar TF, Minev IR, Pietzsch J, Zhang Y, Adv. Sci 2019, 6, 1802077.

[25]. Riley L, Schirmer L, Segura T, Curr. Opin. Biotechnol 2019, 60, 1. [PubMed: 30481603]

[26]. Mealy JE, Chung JJ, Jeong H-H, Issadore D, Lee D, Atluri P, Burdick JA, Adv. Mater 2018, 30, 1705912.

[27]. Shin M, Song KH, Burrell JC, Cullen DK, Burdick JA, Adv. Sci 2019, 6, 1901229.

[28]. Yao B, Wang H, Zhou Q, Wu M, Zhang M, Li C, Shi G, Adv. Mater 2017, 29, 1700974.

[29]. Zhang S, Chen Y, Liu H, Wang Z, Ling H, Wang C, Ni J, Çelebi-Saltik B, Wang X, Meng X, Kim H, Baidya A, Ahadian S, Ashammakhi N, Dokmeci MR, Travas-Sejdic J, Khademhosseini A, Adv. Mater 2020, 32, 1904752.

[30]. Dean DA, Ramanathan T, Machado D, Sundararajan R, J. Electrostat 2008, 66, 165. [PubMed: 19255614]

[31]. Jo H, Sim M, Kim S, Yang S, Yoo Y, Park JH, Yoon TH, Kim MG, Lee JY, Acta Biomater. 2017, 48, 100. [PubMed: 27989919]

[32]. Kishi R, Kubota K, Miura T, Yamaguchi T, Okuzaki H, Osada Y, J. Mater. Chem. C 2014, 2, 736.

[33]. Stie MB, Jones M, Sørensen HO, Jacobsen J, Chronakis IS, Nielsen HM, Carbohydr. Polym 2019, 215, 253. [PubMed: 30981352]

[34]. Hayward W, Haseler L, Kettwich L, Michael A, Sibbitt W Jr, Bankhurst A, Scand. J. Rheumatol 2011, 40, 379. [PubMed: 21469942]

[35]. Agrawal A, Yu HY, Sagar A, Choudhury S, Archer LA, Macromolecules 2016, 49, 8738.

[36]. Wyss HM, Miyazaki K, Mattsson J, Hu Z, Reichman DR, Weitz DA, Phys. Rev. Lett 2007, 98, 238303. [PubMed: 17677943]

[37]. Nih LR, Sideris E, Carmichael ST, Segura T, Adv. Mater 2017, 29, 1606471.

[38]. George PM, Lyckman AW, Lavan DA, Hegde A, Leung Y, Avasare R, Testa C, Alexander PM, Langer R, Sur M, Biomaterials 2005, 26, 3511. [PubMed: 15621241]

[39]. Wu Q, Wei J, Xu B, Liu X, Wang H, Wang W, Wang Q, Liu W, Sci. Rep 2017, 7, 41566. [PubMed: 28134283]

[40]. Spencer AR, Primbetova A, Koppes AN, Koppes RA, Fenniri H, Annabi N, ACS Biomater. Sci. Eng 2018, 4, 1558. [PubMed: 33445313]

[41]. Abidian MR, Daneshvar ED, Egeland BM, Kipke DR, Cederna PS, Urbanchek MG, Adv. Healthc. Mater 2012, 1, 762. [PubMed: 23184828]

[42]. Oh B, Swaminathan V, Malkovskiy A, Santhanam S, McConnell K, George PM, Adv. Sci 2020, 7, 1902573.

[43]. Li L, Ge J, Ma PX, Guo B, RSC Adv. 2015, 5, 92490.

[44]. Roshanbinfar K, Vogt L, Greber B, Diecke S, Boccaccini AR, Scheibel T, Engel FB, Adv. Funct. Mater 2018, 28, 1803951.

[45]. Dong S-L, Han L, Du C-X, Wang X-Y, Li L-H, Wei Y, Macromol. Rapid Commun 2017, 38, 1600551.

[46]. Guo B, Qu J, Zhao X, Zhang M, Acta Biomater. 2019, 84, 180. [PubMed: 30528606]

[47]. Bao R, Tan B, Liang S, Zhang N, Wang W, Liu W, Biomaterials 2017, 122, 63. [PubMed: 28107665]

[48]. Wang W, Tan B, Chen J, Bao R, Zhang X, Liang S, Shang Y, Liang W, Cui Y, Fan G, Jia H, Liu W, Biomaterials 2018, 160, 69. [PubMed: 29396380]

[49]. Dong R, Zhao X, Guo B, Ma PX, ACS Appl. Mater. Interfaces 2016, 8, 17138. [PubMed: 27311127]

[50]. Wu Y, Guo B, Ma PX, ACS Macro Lett. 2014, 3, 1145.

[51]. Shin SR, Aghaei-Ghareh-Bolagh B, Dang TT, Topkaya SN, Gao X, Yang SY, Jung SM, Oh JH, Dokmeci MR, Tang XS, Khademhosseini A, Adv. Mater 2013, 25, 6385. [PubMed: 23996513]

[52]. Navaei A, Saini H, Christenson W, Sullivan RT, Ros R, Nikkhah M, Acta Biomater. 2016, 41, 133. [PubMed: 27212425]

[53]. Cui H, Cui L, Zhang P, Huang Y, Wei Y, Chen X, Macromol. Biosci 2014, 14, 440. [PubMed: 24821672]

[54]. Sawyer SW, Dong P, Venn S, Ramos A, Quinn D, Horton JA, Soman P, Biomed. Phys. Eng. Express 2018, 4, 015005.

[55]. Appel EA, Tibbitt MW, Webber MJ, Mattix BA, Veiseh O, Langer R, Nat. Commun 2015, 6, 6295. [PubMed: 25695516]

[56]. Yu AC, Smith AAA, Appel EA, Mol. Syst. Des. Eng 2020, 5, 401.

[57]. Xu B, Bai T, Sinclair A, Wang W, Wu Q, Gao F, Jia H, Jiang S, Liu W, Mater. Today Chem 2016, 1–2, 15.

[58]. Guarino V, Alvarez-Perez MA, Borriello A, Napolitano T, Ambrosio L, Adv. Healthc. Mater 2013, 2, 218. [PubMed: 23184787]

[59]. Wang L, Wu Y, Hu T, Ma PX, Guo B, Acta Biomater. 2019, 96, 175. [PubMed: 31260823]

[60]. Nune M, Manchineella S, Govindaraju T, Narayan KS, Mater. Sci. Eng. C 2019, 94, 17.

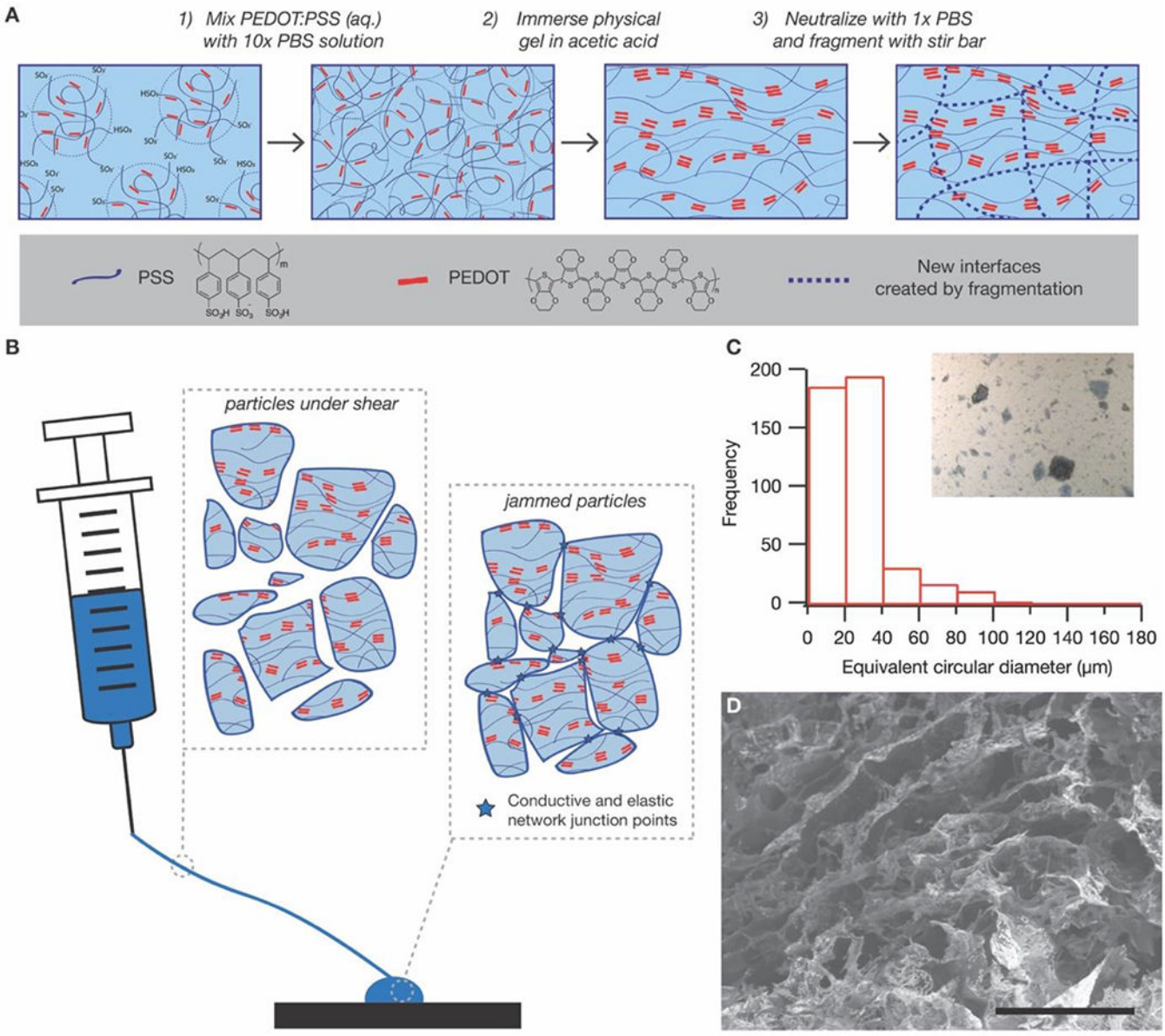

Figure 1.

Fabrication of granular conductive hydrogels. (A) Granular conductive gels are fabricated via a simple three-step process. First, a colloidal gel is formed by mixing PEDOT:PSS solution with concentrated PBS buffer. Second, the colloidal gel is immersed in acetic acid to induce PEDOT aggregation to increase electrical conductivity. Finally, the granular gel is formed by fragmenting the bulk conductive gel with a stir bar. (B) The granular nature of the resultant gel enables the material to flow in response to applied pressure, since microgel particles are not covalently linked and can move past one another. After removal of applied pressure, the particles return to a jammed configuration, with elasticity and conductivity that emerge due to the junctions between jammed particles. (C) Optical microscopy of the granular gel dispersed in water shows that the particles are highly heterogeneous, though with an approximate length scale that is smaller than the inner diameter of a standard 20

gauge needle (603 μm). (Scale bar = 200 μm) (D) Scanning electron microscopy of the lyophilized granular gel confirms the porosity of the hydrogel is retained even after fragmentation. (Scale bar = 50 μm)

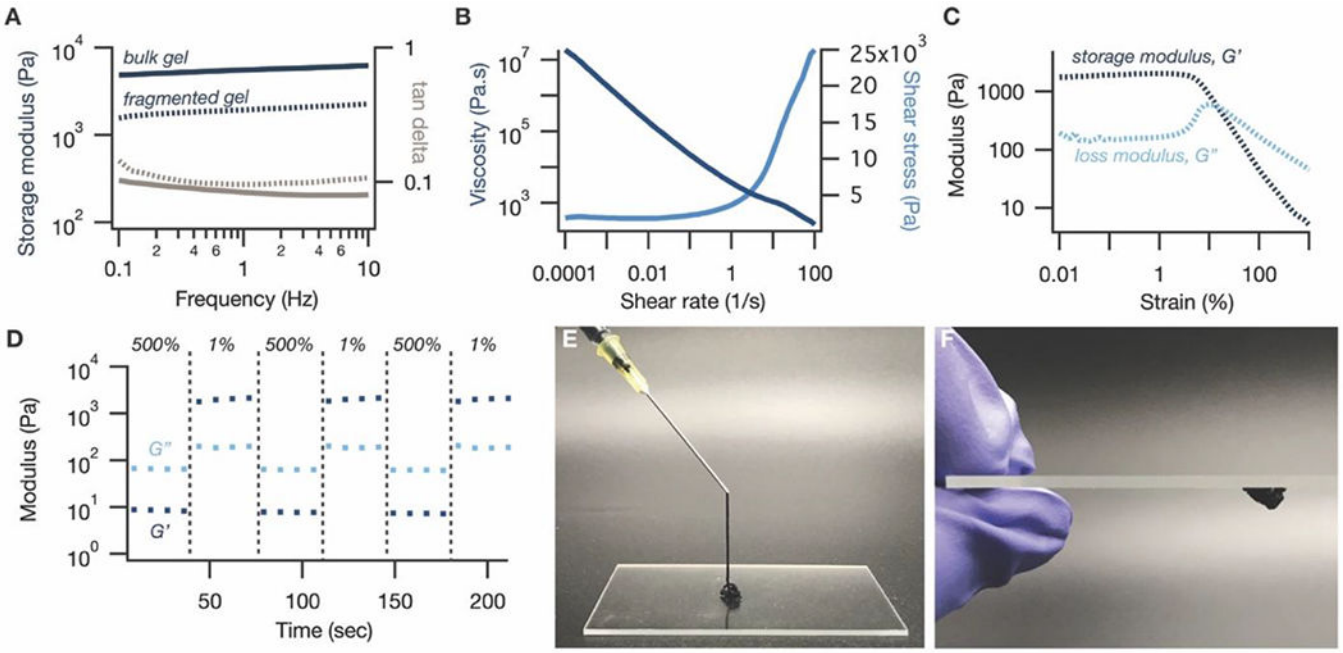

Figure 2.

Rheological properties of granular conductive hydrogels. (A) Fragmentation of the bulk PEDOT:PSS hydrogel results in a slight decrease in storage modulus (blue, dashed line) compared to the bulk gel (blue, solid line), indicating that bond breakage is required to obtain the desired granular structure. Nevertheless, the tan delta of the fragmented gel (gray, dashed line) remains similar and less than 1, indicative of the elasticity that is maintained by the jammed microparticles. (B) The granular gel exhibits clear shear-thinning behavior in its viscosity (dark blue) and shear stress (light blue) profiles, with a power law index of 0.0501, as well as a dynamic yield stress of 1.9 kPa. (C) In an oscillatory shear amplitude sweep, the granular gel exhibits a crossover from solid-like (G', dark blue > G", light blue) to liquid-like (G" > G') behavior at a strain of 15%. The peak in the loss modulus at this point is consistent with a jamming-induced elastic-to-viscous transition. (D) The granular gel is able to quickly and reversibly alternate between liquid-like behavior (G", light blue > G', dark blue) at high strains (500%) and solid-like (G' > G") behavior at low strains (1%). (E) The gel can be injected through a 20 gauge needle and (F) quickly reforms its solid-like elasticity after injection.

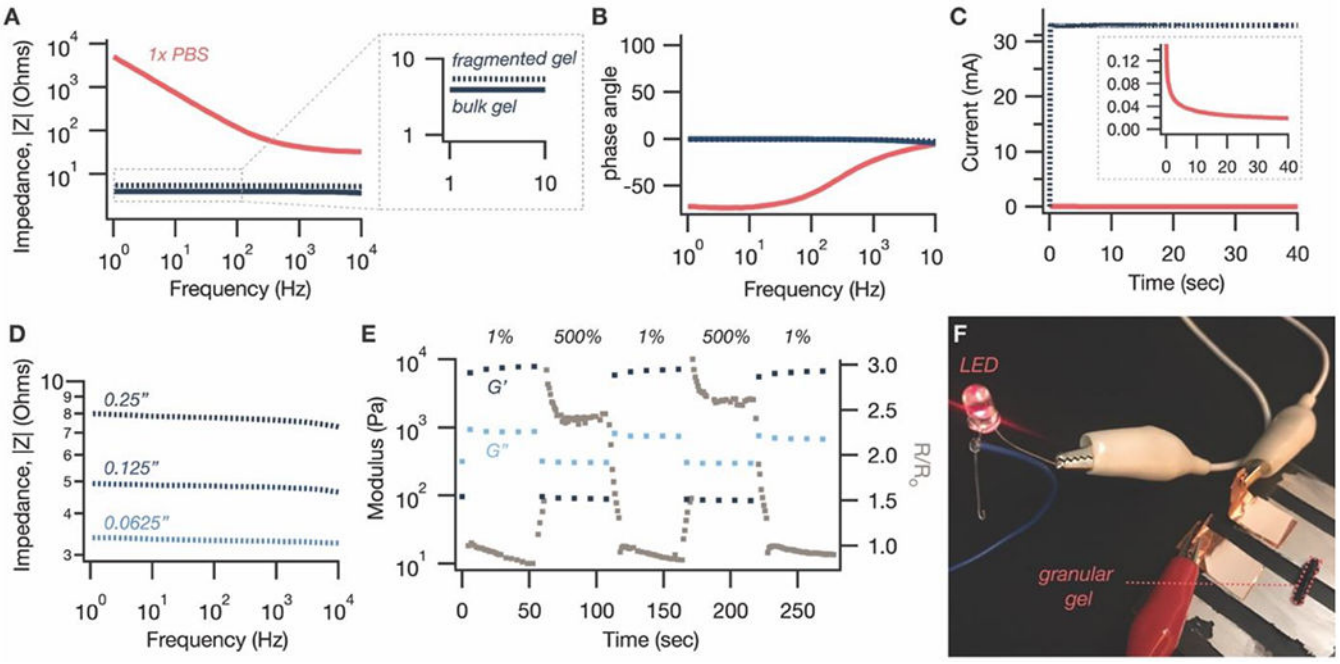

Figure 3.

Electrical properties of granular conductive hydrogels. (A) The impedance of the gel after fragmentation (dashed blue) is slightly higher than before (solid blue). However, the increase is minimal, especially compared to an ionically conductive control of PBS solution (pink). (B) The phase angle of both the fragmented (dashed blue) and bulk (solid blue) conductive gels is near zero, compared to the highly negative phase angle of 1x PBS (pink) at low frequencies. (C) Chronoamperometric measurement of current with the application of a DC voltage of 0.1V confirms that the granular gel (blue) is electrically conductive, with a conductivity of 10.8 S m^{-1}. By comparison, a colloidal PEDOT:PSS gel without acid treatment (pink) draws a small current that rapidly drops off over time. (D) Demonstrating that the improved impedance is not just an interfacial effect, the impedance of the granular gel increases with increasing gap size, consistent with a typical resistor. (E) The resistance across a granular gel sample loaded between two parallel plates (grey squares) tracks its rheological characteristics with the application of high and low strain. This corroborates our hypothesis that the jammed granular microstructure gives rise to macroscopic electrical conductivity in addition to elasticity. (F) Using the granular gel to complete a circuit to light an LED.

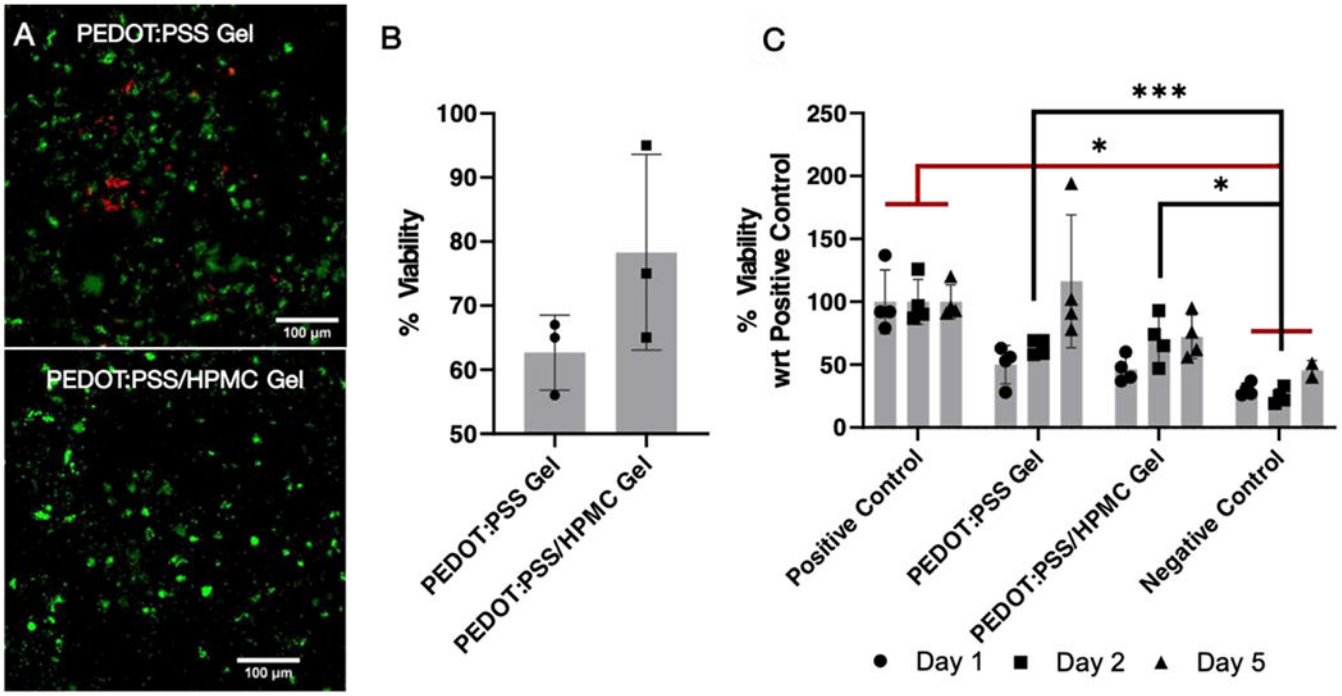

Figure 4.

Cytocompatibility of granular conductive hydrogels. (A) Live/dead assay showing the viability of NPCs within the gel on day 2. (B) Percentage viability of cells encapsulated within the gel matrices determined based on the fluorescence in live/dead assay. The cells within the gel matrices are viable without any significant different between the two groups when analyzed using the t- test. (C) alamarBlue assay illustrates the viability of cells encapsulated within the gel. There was no significant difference between the cells encapsulated within the gel compared to the positive control (cells alone). Negative control is the cells treated with cell lysis solution for 1 hour on day 1 prior to the assay. Cells encapsulated within PEDOT:PSS gel were at least 90% viable compared to the positive control on day 5. Analyzed using a mixed-effects model, followed by Tukey's HSD post hoc test with * $P < 0.05$, **$P<0.01$, ***$P<0.001$. Values represent the mean of independent experiments (N = 4), error bars are S.D.

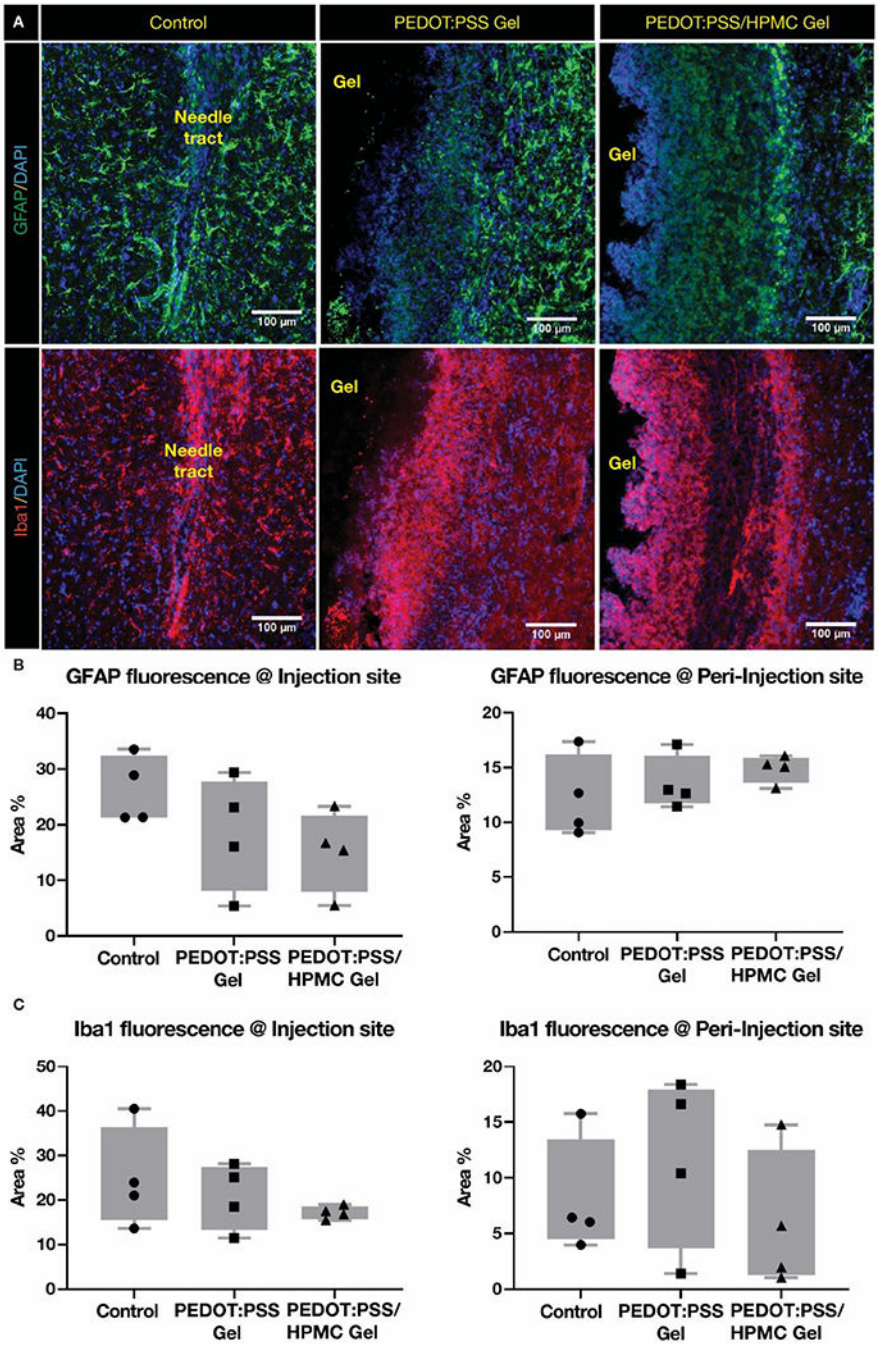

Figure 5.

Inflammatory response post-granular hydrogel injection in rats. (A) Fluorescent images of GFAP (astrocytes) and Iba1 (microglia) staining in rat brain tissue closer to the injection site. The injectable gels are well-formed within the brain tissue and labelled as gel. Percent area under (B) GFAP and (C) Iba1 fluorescence at injection and peri-injection site are quantified. The data demonstrates that the GFAP and Iba1 fluorescence near both the gels

were comparable to that of the control–needle tract without any significant difference between the groups when analyzed through nested 1-way ANOVA.